



A new turbulence model for porous media flows. Part II: Analysis and validation using microscopic simulations

Federico E. Teruel^{a,b,*}, Rizwan-uddin^a

^a Department of Nuclear, Plasma and Radiological Engineering, University of Illinois at Urbana-Champaign, Urbana, IL 61801, USA

^b Centro Atómico Bariloche, CNEA, Bariloche 8400, Río Negro, Argentina

ARTICLE INFO

Article history:

Received 11 August 2008

Received in revised form 2 April 2009

Accepted 2 April 2009

Available online 11 June 2009

Keywords:

Turbulence modeling

Porous media

K - ϵ model

Volume-averaging

ABSTRACT

A new model for turbulent flows in porous media developed in an accompanying paper [F.E. Teruel, Rizwan-uddin, A new turbulence model for porous media flows. Part I: Constitutive equations and model closure, *Int. J. Heat Mass Transfer* (2009), doi:10.1016/j.ijheatmasstransfer.2009.04.017.], in which new definitions of the macroscopic turbulence quantities are introduced, is analyzed and validated. The model is validated using a simple but often used porous medium consisting of a staggered arrangement of square cylinders. Theoretically predicted values of the newly defined turbulence variables, under fully developed conditions, are compared with corresponding variables used in existing turbulence models. Additionally, evolution of the macroscopic turbulence quantities obtained numerically using the model developed here are compared with reference results, obtained by averaging over space the microscopic level solution of the RANS equations. Comparison exercise for the 75% porosity case is carried out for a range of turbulence intensity at the entrance of the porous medium. Comparison of results shows very good agreement. The spatial evolution of the dispersive kinetic energy, which is included in the definition of the macroscopic turbulent kinetic energy introduced here, is computed using the microscopic solution. Its magnitude relative to the conventional turbulent kinetic energy shows the importance of this quantity in the representation of turbulence effects in porous media flows.

© 2009 Elsevier Ltd. All rights reserved.

1. Introduction

A new model for turbulent flow in porous media is developed in Part I of this paper. Reader is referred to Part I for a review of efforts and challenges in modeling turbulent flow in porous media. Focus in Part II is on the equally challenging task of model validation. Since validation of models for turbulent flows in porous media is not a straight forward task, a brief review of the state of the art is given first. This is followed in Section 3 by a summary of the model developed in Part I. The model is next analyzed for fully developed conditions in Section 4. Finally, evaluation of model parameters, simulation results, and comparison with benchmark data are given in Section 5, followed by summary and conclusions in Section 6.

2. Review of efforts to validate turbulence models for porous media

Validation of a model for turbulence in porous media is at least as challenging as, if not more challenging than, developing the model in the first place. To validate, the results obtained using the model are

expected to be compared against experimental data and/or against results obtained using microscopic numerical simulations. Measuring local pointwise data in porous medium at large number of points to allow intermediate scale averaging is not an easy task. Hence, validation of porous media models very often relies on comparison of results against corresponding variables (obtained by area/volume-averaging of the local microscopic results) generated via numerical simulations. However, though this may appear to be a simple task, a practical procedure to validate turbulence models for flow in porous media even against microscopic numerical data has not been established. One of the reasons for this difficulty is the fact that the microscopic results need to be averaged over intermediate scales before the macroscopic model results can be compared against them. This necessitates the microscopic simulation to be carried out over relatively large spaces (due to scale considerations, see Part I). However, when flow over a relatively large porous region with uniform properties is simulated, the porous medium approximation tends to “homogenize” the variables making it difficult to identify a macroscopic variable that shows reasonable spatial variation to allow a meaningful comparison. Note that this dilemma is valid for benchmark data obtained experimentally as well as those generated via microscopic numerical simulations.

Other potential candidate variables, such as the pressure gradient and velocity profile in the spanwise direction, are inappropriate

* Corresponding author. Address: Centro Atómico Bariloche, CNEA, Bariloche 8400, Río Negro, Argentina. Tel.: +54 2944 445166; fax: +54 2944 445299.

E-mail address: teruel@cab.cnea.gov.ar (F.E. Teruel).

Nomenclature

d	square-edge length
f	model function (macroscopic turbulent dissipation rate equation)
F	Forchheimer coefficient
F	Darcy–Forchheimer term
H	REV's dimension (REV volume = $2H \times H$)
I	turbulent intensity
k	macroscopic turbulent kinetic energy (MTKE)
k_{DISP}	dispersive kinetic energy
k_{NK}	space-average of the turbulent kinetic energy
K	permeability
l_m	macroscopic mixing length scale
p	pore length scale
R_i	Darcy–Forchheimer drag force
Re	Reynolds number
U	cross-section averaged streamwise velocity
U_D	V -normalized space-averaged streamwise velocity, Darcy velocity

V_f fluid volume inside the REV

Greek symbols

ε	macroscopic turbulent dissipation rate (MTDR)
ε_{NK}	space-average of the turbulent dissipation rate
ϕ	porosity
ν	kinematic fluid viscosity
ν_T	macroscopic eddy viscosity
ρ	fluid density

Additional notations

$\langle \psi \rangle$	V -normalized space-average of ψ
$\langle \psi \rangle^f$	V_f -normalized space-average of ψ
${}^i\psi$	space fluctuation of ψ
$\overline{\psi}$	used for time-average of ψ or for V_f -normalized space-time average of ψ
ψ'	time fluctuation of ψ
$\overline{\overline{\psi}}$	V_f -normalized space-time average of ψ

due to other reasons. For example, the macroscopic pressure gradient in one-dimensional, fully developed flow in porous media is provided by the Darcy–Forchheimer approximation since the term containing the macroscopic eddy viscosity is identically zero. Therefore, there is no impact of the turbulence quantities on the macroscopic pressure gradient for one-dimensional fully developed flow. And therefore this variable cannot be used to validate the model. The macroscopic velocity profile in a channel filled with porous medium is indeed affected by the eddy viscosity. However, the implementation of the macroscopic model near the system boundaries is not a resolved issue. The porosity in the boundary regions of the system may change and appropriate boundary conditions must be developed for the macroscopic turbulence quantities before it can be used for validation purposes.

Possibly due to reasons discussed above, rigorous model validation is not reported for most new turbulence models for flow in porous media. Based on numerical calculations carried out using the k - ε model Kuwahara et al. [1] showed that the Darcy–Forchheimer law can be employed in the turbulence regime for steady, fully developed flows. Later, Nakayama and Kuwahara [2] considered a steady, unidirectional, macroscopic flow entering a semi-infinite periodic array of square rods to validate their turbulence model for porous media. This model is referred to as the NK model. They compared the spatial evolution of the macroscopic turbulence quantities obtained from both, the microscopic and macroscopic, simulations for the 75% porosity case. Although the agreement is in general good (errors are below 30%), only one set of macroscopic boundary conditions was considered for the 75% porosity case. Pedras and de Lemos [3] extensively investigated the characteristics of the model they developed under different physical conditions [4]. However, possibly because of the difficulties identified above, there is rather limited attempt to validate the model. Results obtained using this model [3] have been compared against the microscopic results in a manner similar to the validation exercise carried out for the NK model.

The analysis and validation exercise for the model developed in Part I is restricted by the same limitations that applied to earlier models. In the first part of this model validation exercise, theoretically predicted macroscopic turbulence quantities for fully developed flow in a porous medium consisting of square rods placed in a staggered array are compared against those computed numerically by Nakayama and Kuwahara [2]. This comparison is used to understand and quantify the difference between present definitions of

the macroscopic turbulence quantities and those employed in other models.

The second part is devoted to the determination of model parameters and validation of the turbulence model in porous media. A numerical experiment similar to the one carried out by Nakayama and Kuwahara [2] is carried out to validate the spatial evolution of macroscopic turbulence quantities predicted by the model. However, different from [2], different sets of macroscopic boundary conditions, that are calculated based on microscopic solutions, are simulated. The RANS equations (microscopic simulation) are solved for the case of a unidirectional flow entering the porous medium considered in this study. The spatial evolution of the relevant macroscopic quantities can then be obtained by appropriate averaging of the microscopic results. Macroscopic porous media turbulence equations are also solved for the same problem. Results obtained using the latter approach are compared with those obtained using the microscopic simulations. The numerical experiment is useful not only to test if the model can capture the salient features of turbulence in porous media but also to study the relevance of the dispersive kinetic energy in the macroscopic representation of turbulence in porous media.

3. Macroscopic turbulence model

The characteristic features of the new model are summarized in this section. Refer to Part I for details. A novel definition of the space-time fluctuation in porous media form the basis of the new macroscopic turbulence model developed in Part I [5]. The fluctuations in this model are defined with respect to space-time averaged quantities. For any flow variable ψ , the following decomposition is introduced [5]:

$$\psi(r, t) = \overline{\overline{\psi}}(r, t) + \psi''(r, x, t), \quad (1)$$

with this definition of the fluctuation, the macroscopic turbulent kinetic energy (MTKE, k) is defined as:

$$k = \frac{\overline{\overline{u_j'' u_j''}}}{2} = \frac{\langle \overline{u_j'' u_j''} \rangle^f}{2} + \frac{\langle \overline{u_j^i u_j^i} \rangle^f}{2} = k_{\text{NK}} + k_{\text{DISP}}, \quad (2)$$

showing that k is equal to the space-average of the microscopic TKE (k_{NK}) plus the dispersive kinetic energy (k_{DISP}) or the trace of the space dispersion of the mean (time-average) flow. Similarly, the

macroscopic turbulent dissipation rate (MTDR) is naturally defined in the new model as:

$$\varepsilon = v \frac{\overline{\partial u_i'' \partial u_i''}}{\partial x_j \partial x_j} = v \left\langle \frac{\partial u_j'' \partial u_j''}{\partial x_j \partial x_j} \right\rangle^f + v \left\langle \frac{\partial^j \bar{u}_i \partial^j \bar{u}_i}{\partial x_j \partial x_j} \right\rangle^f = \varepsilon_{NK} + v \left\langle \frac{\partial^j \bar{u}_i \partial^j \bar{u}_i}{\partial x_j \partial x_j} \right\rangle^f, \quad (3)$$

where ε_{NK} is the space-average of the microscopic turbulent dissipation rate (TDR).

The complete set of equations for the macroscopic model is given in Reference [5]. For the case of isotropic and constant porosity porous medium, the two-equation model is given by:

$$\frac{\partial \bar{u}_i}{\partial x_i} = 0, \quad (4)$$

$$\frac{D \bar{u}_i}{Dt} = -\frac{1}{\rho} \frac{\partial (\bar{p} + 2/3k)}{\partial x_i} + \frac{\partial}{\partial x_j} \left[(v + v_T) \frac{\partial \bar{u}_i}{\partial x_j} \right] + R_i, \quad (5)$$

$$\frac{Dk}{Dt} = -\overline{u_j'' u_j''} \frac{\partial \bar{u}_i}{\partial x_j} + \frac{\partial}{\partial x_j} \left[\left(v + \frac{v_T}{\sigma_k} \right) \frac{\partial k}{\partial x_j} \right] - \varepsilon - \bar{u}_i R_i, \quad (6)$$

$$\frac{D\varepsilon}{Dt} = -C_{\varepsilon 1} \frac{\varepsilon}{k} \overline{u_j'' u_j''} \frac{\partial \bar{u}_i}{\partial x_j} + \frac{\partial}{\partial x_j} \left[\left(\frac{v_T}{\sigma_\varepsilon} + v \right) \frac{\partial \varepsilon}{\partial x_j} \right] - C_{\varepsilon 2} \frac{\varepsilon^2}{k} + f(\phi, K) \frac{\varepsilon \sqrt{\bar{u}_j \bar{u}_j}}{\sqrt{K}}, \quad (7)$$

with:

$$R_i = -\frac{\phi v}{K} \bar{u}_i - \frac{\phi^2 F}{\sqrt{K}} \sqrt{\bar{u}_j \bar{u}_j} \bar{u}_i, \quad (8)$$

$$\overline{u_i'' u_j''} = -v_T \left(\frac{\partial \bar{u}_i}{\partial x_j} + \frac{\partial \bar{u}_j}{\partial x_i} \right) + \frac{2k}{3} \delta_{ij}, \quad v_T = C_\mu \frac{k^2}{\varepsilon}.$$

4. Model characteristics under fully developed conditions

In general, to simulate turbulent flows in porous media, not only the model parameters but also the fully developed (equilibrium) values of the macroscopic turbulence quantities must be specified (e.g. [2]). In the present model and for a particular porous medium, in addition to the permeability and the pressure gradient (i.e., Darcy–Forchheimer approximation), the model parameters and the values of the fully developed MTKE must be specified to solve the two-equation model developed in Part I. The latter can be obtained, for example, from the one-equation model. The procedure to evaluate the fully developed values of the MTKE using the one-equation model is described in this section for a geometry that has been widely used to study turbulence in porous media (e.g. [2,4]). First, fully developed (equilibrium) turbulence quantities analytically predicted by the one and two-equation models are determined as a function of porosity. Second, analytically predicted values are compared against those calculated numerically (e.g. [2]).

4.1. Analytical estimates for fully developed values

A simple 2D geometry consisting of a staggered arrangement of square cylinders is considered (Fig. 1). The flow, from left to right, is incompressible and fully developed in the macroscopic sense; that is the intrinsic fluid velocity is one dimensional. The edge size

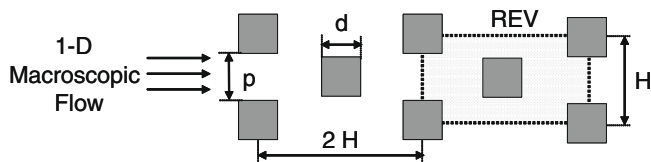


Fig. 1. Simple porous media formed by staggered square cylinders.

of each cylinder is d and the distance between cylinder's centers is H . The distance $p (=H - d)$ is used as a measure of the pore size. The size of the square rods is varied from 0 to H to allow variation in the porosity. Distance between square rods in the vertical direction, H , is fixed.

Variables are normalized with the cell length scale (H) and the volume-averaged velocity (Darcy fluid velocity, $U_D = Up/H$, where U is the average inlet streamwise velocity over the cross-section p). The dimensionless variables and parameters are,

$$\varepsilon^* = \frac{\varepsilon H}{U_D^3} \quad k^* = \frac{k}{U_D^2} \quad Re = \frac{U_D H}{\nu} \quad \frac{p}{H} = 1 - \sqrt{1 - \phi}. \quad (9)$$

Note that constant Re implies constant mass flow rate and the ratio between the pore length scale and the distance between rods has been written as a function of porosity. Furthermore, the porous matrix shown in Fig. 1 has been shown to obey the modified Ergun relationship (valid in general for packed beds only [6]) if appropriate constants are employed. Based on numerical experiments, Kuwahara et al. [1,7,8], characterized the Darcy–Forchheimer approximation for the porous matrix under consideration relating the Forchheimer constant (F) and the permeability (K) to porosity as follows [8]:

$$F = \frac{1}{\sqrt{30}\phi^{3/2}}, \quad K = \frac{\phi^3}{120(1 - \phi)} H^2. \quad (10)$$

Expressions for the permeability and Forchheimer constant are valid in the 10–80% [7] and 45–85% porosity range, respectively [8].

Based on the microscopic analysis it is assumed that the mixing length scale is of the order of the largest eddy within the porous matrix ($\approx p$). This assumption was also made by Antohe and Lage [9]. However, any factor of the pore length scale may be used. Therefore, the ratio between the permeability and the mixing length scale appearing in the definition of f (Eq. 53 in Part I) can be written as a function of porosity only,

$$\frac{f^2}{K} = \frac{p^2}{K} = \frac{120}{\phi^3} \left(\sqrt{1 - \phi} + \phi - 1 \right)^2. \quad (11)$$

Note that $K = K(\phi)$. The fully developed, dimensionless, macroscopic turbulence quantities as a function of porosity are therefore given by:

$$\varepsilon_\infty^* = \frac{120\sqrt{1 - \phi}}{\phi^4} \left[\frac{\sqrt{1 - \phi}}{Re} + \frac{1}{60} \right], \quad (12)$$

$$k_\infty^* = \left(\frac{120}{C_D} \frac{(\sqrt{1 - \phi} + \phi - 1)}{\phi^4} \left[\frac{\sqrt{1 - \phi}}{Re} + \frac{1}{60} \right] \right)^{2/3}. \quad (13)$$

Note that because expressions for the permeability and the Forchheimer constant have been employed to derive Eqs. (11)–(13), these equations should be considered valid in the 45–80% porosity range. However, these quantities will be plotted over 10–90% porosity range in the next section, where they are compared with numerically simulated results, to show the trend beyond the validity range.

4.2. Comparison of analytical estimates for fully developed values with numerical results

Numerical results presented in Nakayama and Kuwahara [2], obtained by averaging the microscopic simulation results of high Reynolds number flows in the geometry shown in Fig. 1 (2D, $k-\varepsilon$ model with wall functions), cover the porosity range of [0.2–0.85] and are fairly independent of Reynolds number [10^5 – 10^7]. Nakayama and Kuwahara [2] fitted the macroscopic turbulence quantities to correlations with porosity as the parameter. Although the definitions of the macroscopic turbulence quantities

introduced here differ from those in NK's model, it is of interest to compare them. The results for the one-equation model presented here are shown for $Re = 10^6$. Fig. 2 shows the steady state values of the fully developed MDR (2a) and the MTKE (2b) for the one-equation model for three different values of C_D as a function of $(1 - \phi)\phi^{1/2}$ and $(1 - \phi)^2/\phi$, respectively, choices dictated by [2]. NK's correlations are also plotted for comparison. Horizontal arrow indicates the reported porosity-range over which numerical experiments were carried out by NK.

Recalling the relationship between the macroscopic turbulence quantities defined here and those defined by Nakayama and Kuwahara (k_{NK} and ε_{NK}):

$$\varepsilon = \varepsilon_{NK} + \nu \left\langle \frac{\partial^i \bar{u}_i}{\partial x_j} \frac{\partial^j \bar{u}_i}{\partial x_j} \right\rangle^f \quad \text{for fully developed flow} \quad \varepsilon_{NK} + \nu \left\langle \frac{\partial \bar{u}_i}{\partial x_j} \frac{\partial \bar{u}_i}{\partial x_j} \right\rangle^f, \quad (14)$$

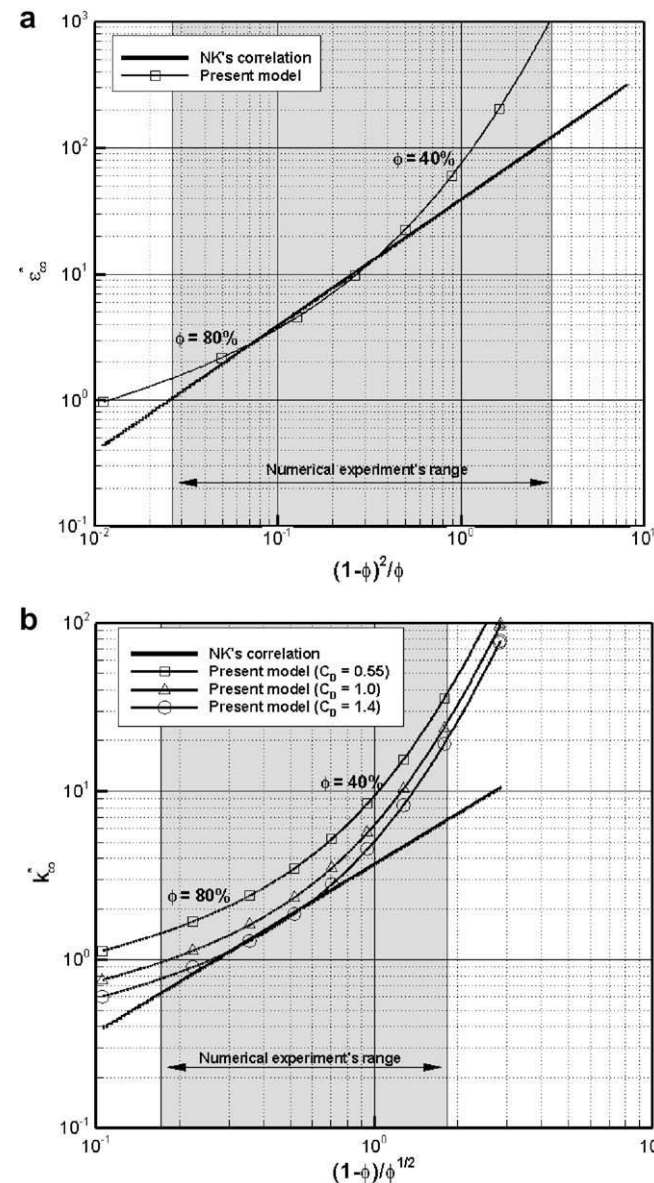


Fig. 2. Comparison of numerical experiments and values predicted by the model for fully developed macroscopic turbulence quantities as a function of porosity. Note that symbols are for every 10% increment in porosity. (a) MDR predicted by the model and NK's correlation. (b) MTKE predicted by the one-equation model and NK's correlation.

and

$$k = k_{NK} + \frac{\langle \bar{u}_i^j \bar{u}_i^j \rangle^f}{2}, \quad (15)$$

a significant deviation between the two might be expected at least under certain conditions. For the macroscopic dissipation rate, Eq. (14) shows that the present definition of the MDR under fully developed conditions is the sum of the space-average of the turbulent dissipation rate and the space-average of the dissipation of the mean flow (or time-averaged flow). As the latter quantity is of the order Re^{-1} with respect to the turbulent dissipation rate [10], it is expected that $\varepsilon \rightarrow \varepsilon_{NK}$ for large Re numbers. Fig. 2a shows good agreement between these two quantities for the intermediate range of porosity, $0.5 < \phi < 0.8$ or $0.05 < (1 - \phi)^2/\phi < 0.5$. As mentioned earlier, for porosities outside this range, the validity of the expression employed to approximate the Darcy–Forchheimer drag force in the present porous media model (Eq. (10)) is questionable and therefore any agreement would have been fortuitous.

The MTKE (Eq. (15)) is composed of k_{NK} plus the dispersive kinetic energy. The latter quantity is expected to be a significant fraction of the MTKE at lower porosities, independent of the Re number. Fig. 2b shows that over the intermediate range of porosity, $0.5 < \phi < 0.8$ or $0.22 < (1 - \phi)/\phi^{1/2} < 0.71$, the MTKE predicted by the one-equation model shows a dependence on the porosity that is similar to that shown by the numerically calculated k_{NK} . MTKE is shown for three values of the model parameter, C_D : 0.55, 1.0 and 1.4. This constant, which determines the level of the MTKE (Fig. 2b), can be determined, for instance, by carrying out numerical experiments for a particular porosity. *A priori*, there is no reason to believe that the value of C_D most suitable for clear flows (i.e., $C_D = 0.55$) will also be most appropriate for porous media flows.

Thus, it is clear that the MTDR (ε) for high Re number flows under fully developed conditions, as defined in the present model as well as that employed in other models (e.g., NK's and Pedras and de Lemos [3]), can be determined by means of the pressure drop (in the REV) as it is dictated by the theoretical model. Additionally, for a given porous medium where the drag forces in the momentum equation are known, the MTKE under fully developed conditions calculated using the one-equation model can be used to supplement the two-equation model.

5. Model characteristics under developing conditions: determination of model parameters and model validation

A numerical experiment similar to the one carried out by Nakayama and Kuwahara [2] is carried out in this study to determine the model parameters and to validate the model. The RANS equations (microscopic simulation) are solved for the case of the unidirectional flow entering the porous medium shown in Fig. 1 (Section 5.1). The spatial evolution of the relevant macroscopic quantities is then obtained in Section 5.2 by space-averaging the microscopic results. These serve as reference results. Macroscopic equations are also solved for the same problem and the macroscopic results are then compared with the corresponding variables obtained using the microscopic simulations.

The fact that the macroscopic turbulence quantities, such as the MTKE and MDR, are significantly different from those defined for clear flows (i.e., macroscopic quantities are quantities averaged in space) suggests that model parameters introduced in the macroscopic model ($C\varepsilon_1, C\varepsilon_2, C_{\mu}, \sigma_k, \sigma\varepsilon$; see Eqs. (4)–(8)) may differ significantly from corresponding parameters usually found in models for clear flows. Moreover, model parameters may also depend on the geometry of the porous medium. Therefore, in this study, model parameters are determined by minimizing the difference between the macroscopic and space-time averaged microscopic results.

Additionally, as model parameters should be independent of the boundary conditions, the minimization process is carried out over a space of different sets of boundary conditions. Details are given in Section 5.3.

5.1. Microscopic simulations of turbulent flow in the porous medium

Schematic diagram of the domain selected for simulation and comparison is shown in Fig. 3. The fluid flows from left to right, entering the porous medium after flowing a distance of $2H$ as clear flow. The porous medium extends for a distance of $16H$ (i.e., eight REV in a row). To save computational time, and based on the fact that simulations of the REV at high Re numbers with periodic boundary conditions result in symmetric results (steady solutions [11], see also [2]), only the bottom half of the REV ($H/2$) is simulated.

SIMPLER algorithm developed by Patankar [12] is used to solve the RANS equations. Central difference and the QUICK scheme [13,14] are employed to, respectively, model the diffusion and the convective terms. Crank–Nicholson or the backward Euler scheme is used to advance in time. The k – ε model with near wall treatment developed by Abe et al. [15] is used to model the Reynolds stresses. The solver has been fully tested and validated for geometries including those presented in this study as well as for a large range of Reynolds numbers. Additional details are available in Ref. [11]. Results reported here were found to be independent of any further grid refinement [11]. The non-uniform but structured grid resolution employed for each REV, shown in Fig. 3, was 192×48 (streamwise \times vertical direction). Uniform profiles of the relevant quantities in the entire domain are used as initial conditions.

The Re number is set at 10^4 and only the case of 75% porosity is presented here. A total of six simulations, corresponding to six different boundary conditions (BCs) at the inlet were carried out. Although the inlet velocity profile is the same for each simulation, the turbulence intensity at the inlet was varied to obtain different flow distributions in the porous medium and, consequently, different macroscopic solutions. Table 1 shows selected inlet boundary values for each turbulence quantity simulated, as well as the corresponding turbulence intensity and the ratio of the eddy viscosity to the fluid viscosity that resulted for each set. [Additional details of the BCs chosen in this study are given in Appendix A.]

It is important to note that the macroscopic boundary conditions at the inlet in this study are calculated based on the solutions of the RANS equations. The macroscopic inlet boundary conditions are evaluated by space-averaging the microscopic solution in the first REV defined inside the porous medium (see Fig. 3). Note that although any macroscopic boundary condition may be imposed on

Table 1

Microscopic turbulence quantities for six sets of inlet boundary conditions.

BC	k	ε	I (%)	ν_T/ν
Set 1	1.00E-05	3.16E-08	0.26	2.8
Set 2	1.00E-04	1.00E-06	0.8	9.0
Set 3	1.00E-03	3.16E-05	2.6	28.5
Set 4	1.00E-02	1.00E-03	8.2	90.0
Set 5	1.00E-01	3.16E-02	25.8	284.6
Set 6	5.00E-01	3.54E-01	57.7	636.4

the macroscopic model, this does not assure that the imposed values are actually realizable in an experiment.

5.1.1. Microscopic results and expectations for macroscopic behavior

Though the purpose of the microscopic simulations is to generate a set of reference macroscopic results (by space-averaging the microscopic results) against which the macroscopic results obtained using the model can be compared, nevertheless, it is important to outline the salient features of the microscopic spatial evolution of the flow in the porous medium to facilitate the understanding of the space-averaged values presented later. Fig. 4 shows the distribution of the TKE (a), the distribution of the TDR (b) and the streamlines of the mean flow in (c), for Set 1 of BCs given in Table 1. The spatial evolution of the TKE—which for this set of BCs is low at the entrance (blue color) relative to the fully developed level (red color)—is determined by the flow interaction with the walls, and reaches its equilibrium value inside the REV. The volume-average of the TKE is hence expected to evolve from a low value at the inlet to a larger fully developed one. Thus, the MTKE, as defined in this study, is not only dependant on the volume-average of the TKE but also on the trace of the hydrodynamic dispersion of the mean flow. Interpretation of this quantity is facilitated by considering the REV's shown in Fig. 4(c). The first REV that the fluid passes through (top) shows a more complex distribution of eddies than the REV downstream where the conditions are fully developed (bottom). Therefore, the dispersive kinetic energy is larger in the entrance region, and it is expected to decay to a constant lower value downstream. The close relationship between the TKE and the distribution of the mean flow inside the REV is expected to be captured by the definition of the MTKE in the model developed in Part I.

Insight in the macroscopic dissipation rate can be also be gained by analyzing the spatial evolution of the microscopic turbulence dissipation rate. Here it is worth recalling the fact that the dissipation of the mean flow is relatively small compared to the turbulence dissipation rate at this Re number. The turbulence dissipation rate evolves in a fashion similar to that of the TKE. Thus, the macroscopic TDR appears to increase monotonically to its equilibrium value.

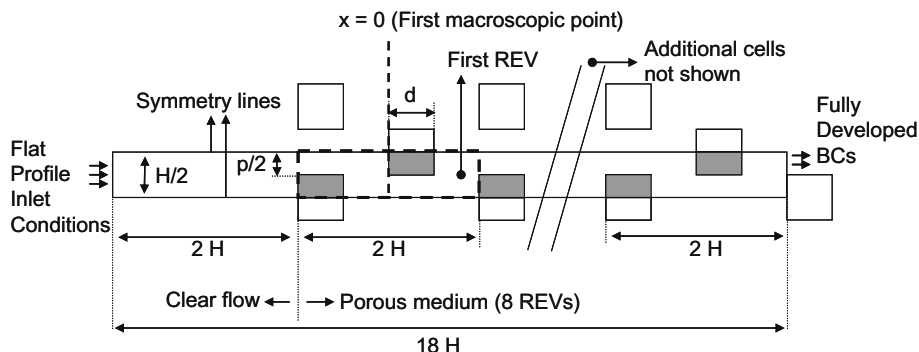


Fig. 3. Geometry of the domain simulated for the case of a free stream entering the porous medium ($18H \times H/2$).

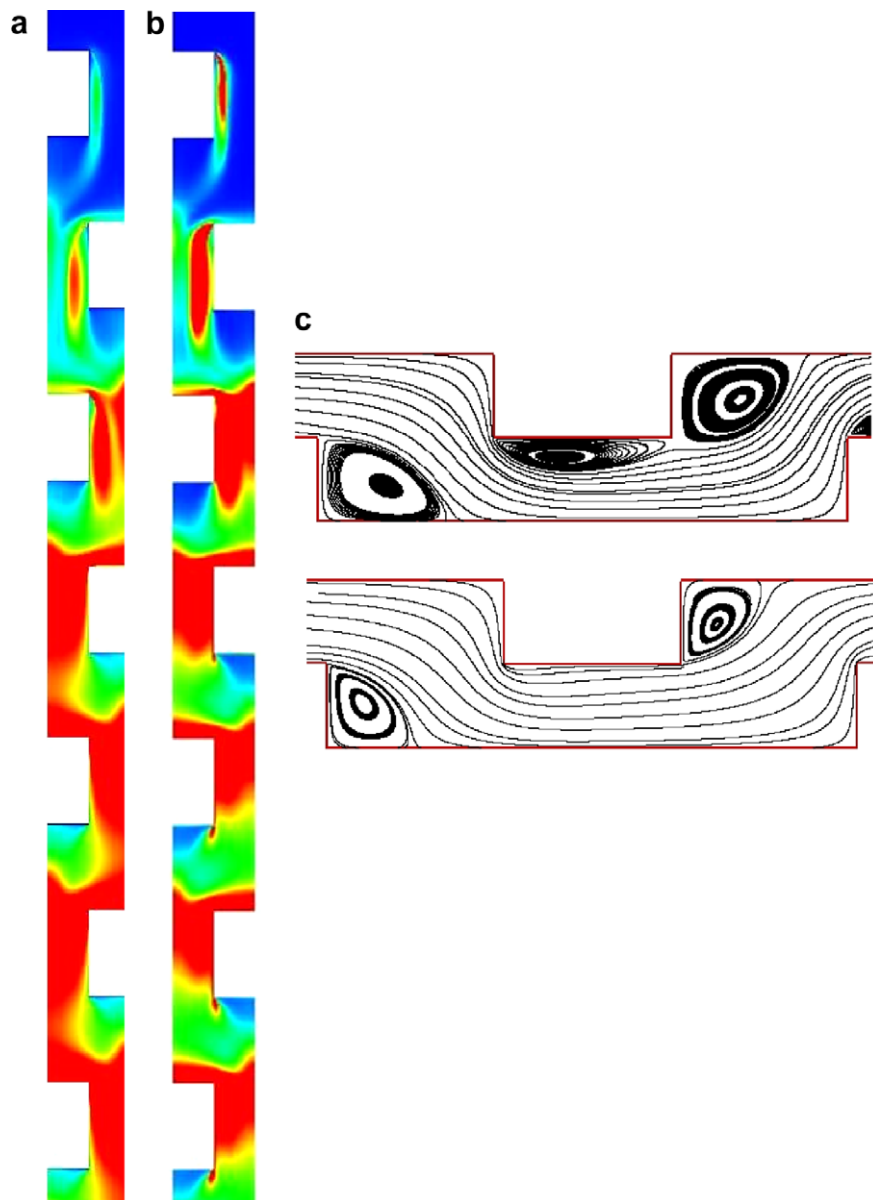


Fig. 4. Distribution of the microscopic TKE (a) and TDR (b) (the fluid is flowing from top to bottom). Blue and red colors correspond to nondimensional levels of 0.0 and 0.25, respectively. Streamlines for two REV's are shown in (c). The top panel corresponds to the first REV in the domain, and the bottom one shows the fully developed condition. These results are for BC Set 1. (For interpretation of the references to color in this figure legend, the reader is referred to the web version of this paper.)

5.2. Averaging the microscopic variables

As pointed out by Gray et al. [16], a precise identification of different scales in a particular system is very difficult, and no precise criterion exists for this purpose. As a general criterion, the scale of the REV should be such that the averaged quantity is fairly insensitive to small changes in the size of the averaging volume. Additionally, it should not be dominated by the fluctuations at the pore scale nor smoothed over the global scale of the system. The flow characteristics in the streamwise direction shown in Fig. 4 suggest that the large scale of the system is approximately $10H$ (i.e., no variation is found beyond this scale). The small scale of the system is approximately given by the size of the square edge (d) or the vertical distance between the squares (p). These length scales are unfortunately not much smaller than H . Therefore, in this problem, the scale separation is not naturally well defined. However, as the volume-averaged quantities behave rather well for an intermediate scale ($\sim 2H$), the comparison between the mac-

roscopic model results and the spatial average of the microscopic results is carried out over this scale. This choice is assessed in Ref. [11], where an extensive study of the behavior of the macroscopic quantities as a function of the REV's size is carried out. In addition, it should be noted that the cell averaging has been shown to be sufficient for periodic structures [17].

The spatial evolution of the macroscopic turbulence quantities is then computed by averaging the microscopic solution over the REV ($2H$). The macroscopic solution thus obtained will be considered the "reference" or "benchmark" solution against which the results of the macroscopic model will be compared. As the microscopic solution was obtained based on a time-averaged simulation (RANS equations), the macroscopic variables also need to be expressed as a function of time-averaged quantities.

The definition of the MTKE introduced in Part I is simply the total kinetic energy minus the filtered kinetic energy (see Eq. (15)). Explicitly, if the REV is discretized into discrete cells (or control volumes) and k_{ij} is the TKE in the cell ij calculated from the

microscopic simulations, then k can be expressed in terms of the variables that can be obtained from the microscopic simulations, as (note the term that corresponds to k_{NK}):

$$k \cong \underbrace{\frac{1}{2H^2\phi} \sum_{ij} k_{ij} C_{ij}}_{k_{\text{NK}}} + \frac{1}{2} \frac{1}{2H^2\phi} \sum_{ij} (\overline{u_{ij}u_{ij}} + \overline{v_{ij}v_{ij}}) C_{ij} - \frac{1}{2} \left(\frac{1}{2H^2\phi} \right)^2 \left[\left(\sum_{ij} \overline{u_{ij}C_{ij}} \right)^2 + \left(\sum_{ij} \overline{v_{ij}C_{ij}} \right)^2 \right], \quad (16)$$

where the volume of each cell is C_{ij} , $2H^2\phi$ is the fluid volume of the REV, and $\overline{u_{ij}}$ and $\overline{v_{ij}}$ are the streamwise and vertical components of the mean velocity vector, respectively. In a similar fashion, the macroscopic dissipation rate (MDR, ε) introduced in Part I can be expressed in terms of the variables computed in the microscopic solution. Based on the definition of the MDR, it is noted that for fully developed macroscopic flow, Eq. (14) holds. The MDR can be computed using the RANS solution as:

$$\varepsilon \cong \underbrace{\frac{1}{2H^2\phi} \sum_{ij} \varepsilon_{ij} C_{ij}}_{\varepsilon_{\text{NK}}} + \nu \frac{1}{2H^2\phi} \times \sum_{ij} \left(\frac{\partial \overline{u_{ij}}}{\partial x} \frac{\partial \overline{u_{ij}}}{\partial x} + \frac{\partial \overline{u_{ij}}}{\partial y} \frac{\partial \overline{u_{ij}}}{\partial y} + \frac{\partial \overline{v_{ij}}}{\partial x} \frac{\partial \overline{v_{ij}}}{\partial x} + \frac{\partial \overline{v_{ij}}}{\partial y} \frac{\partial \overline{v_{ij}}}{\partial y} \right) C_{ij}, \quad (17)$$

where ε_{ij} is the dissipation rate in the ij -th control volume.

Before proceeding to the macroscopic results, a point related to the Darcy–Forchheimer approximation and the evaluation of the pressure gradient in the developing flow region is briefly discussed. The Darcy–Forchheimer approximation depends only on the macroscopic velocity and on the properties of the porous medium. Therefore, a constant driving force, or equivalently a constant pressure gradient, is expected in the porous region of the problem under consideration. However, results reported in Ref. [11] show that for the turbulent flow in the porous medium analyzed here, the drag forces do vary in the developing region. Since the objective here is to evaluate the behavior of the macroscopic turbulence quantities irrespective of the choice made to describe the drag forces in the momentum equation, the Darcy–Forchheimer approximation is not employed in the macroscopic model and the macroscopic pressure gradient is evaluated from the microscopic results. [Note that the approach followed to develop the model in this study [5] allows the use of any expression to describe the drag forces in the momentum equation.] To avoid oscillations due to volume-averaging, the spatial derivative of the macroscopic pressure gradient is calculated as:

$$\frac{d}{dx} P \Big|_{x_0} = \frac{P(x_0 + H) - P(x_0 - H)}{2H}, \quad (18)$$

where P is the space-time averaged pressure.

5.3. Macroscopic turbulence quantities

The results of the macroscopic turbulence model developed in Part I are compared with the macroscopic “benchmark” results obtained in the previous section. The set of equations that describe the macroscopic model in 1D is written as:

$$\frac{1}{\phi} \frac{dk^*}{dx^*} = \frac{d}{dx^*} \left[\left(a \frac{k^{*2}}{\varepsilon^*} + \frac{1}{\text{Re}} \right) \frac{dk^*}{dx^*} \right] - \varepsilon^* - U^* \frac{dP^*}{dx^*}, \quad (19)$$

$$\frac{1}{\phi} \frac{d\varepsilon^*}{dx^*} = \frac{d}{dx^*} \left[\left(b \frac{k^{*2}}{\varepsilon^*} + \frac{1}{\text{Re}} \right) \frac{d\varepsilon^*}{dx^*} \right] - c \frac{\varepsilon^{*2}}{k^*} + c \frac{\varepsilon_{\infty}^*}{k_{\infty}^*} \varepsilon^*, \quad (20)$$

where dP^*/dx^* will be calculated from the microscopic numerical results. The model parameters— a , b and c —need to be determined.

Note that the values of the corresponding model parameters for the clear flow case are unlikely to be applicable to the porous media case.

5.3.1. Evaluation of model parameters

The corresponding values of the parameters in the standard k – ε model for the clear flow equations are: $a = C_{\mu}/\sigma_k = 0.09$, $b = C_{\mu}/\sigma_{\varepsilon} = 0.069$ and $c = C_{\varepsilon_2} = 1.92$. These values are expected to be significantly different for the porous media model. For example, the microscopic level molecular diffusion, turbulent diffusion and dispersion in the transverse direction, may enhance the diffusion (coefficients a and b) in the streamwise direction at macroscopic scales [This effect is clearly exemplified by the Taylor–Aris dispersion.]. To estimate the three constants for the porous medium under study (with a uniform porosity and constant Re number), it is assumed that these coefficients are independent of the inlet BCs. Six microscopic simulations are carried out with six different boundary conditions. Following the procedure described in the previous section, reference macroscopic solutions are obtained from these microscopic results. Solutions obtained using the macroscopic model (Eqs. (19) and (20)) with different sets of parameters (a , b and c) are then compared with the reference solutions. The parameters are then estimated by minimizing the error for all six cases.

For each microscopic simulation corresponding to the inlet boundary conditions in Fig. 3 (Table 1), microscopic results are integrated in the first (inlet) REV of the porous medium to yield an inlet macroscopic boundary condition for the macroscopic model. Additionally, the fully developed macroscopic values are computed using Eqs. (16) and (17) to be used as the boundary condition at the exit for the macroscopic model. Table 2 shows values thus computed for different macroscopic inlet BCs.

Values tabulated in Table 2 are used as boundary values to numerically solve the macroscopic model Eqs. (19) and (20) over a domain that extends from $x/H = 0$ to $x/H = 14$, using a non-uniform grid with a total of 1000 grid points (geometric grid; finer grid at the inlet; geometric ratio = 1.0015). Diffusion terms are approximated with central differences and the convective term with the first order upwind scheme. The system of equations is solved using an LU decomposition as a boundary value problem for each turbulence variable in a segregated scheme. Results are tested to be independent of the location of the outlet boundary condition and grid size.

The volume-averaged results of the microscopic solution are interpolated (linearly) on to the macroscopic grid and compared to the macroscopic solution obtained for each set of model parameters. A relative quadratic error is defined for each inlet BC and each set of parameters as:

$$\text{error}_j(a, b, c) = \frac{1}{N} \sum_i^N (k_{\text{macro}}(i)/k_{\text{micro}}(i) - 1)^2 + (\varepsilon_{\text{macro}}(i)/\varepsilon_{\text{micro}}(i) - 1)^2, \quad (21)$$

Table 2

Macroscopic turbulence quantities at the inlet and outlet, computed for each set of microscopic BCs.

Microscopic inlet BCs	Macroscopic BCs (75% porosity)					
	Inlet		Inlet/outlet		Outlet	
	k^*	ε^*	k^*/k_{∞}^*	$\varepsilon^*/\varepsilon_{\infty}^*$	k_{∞}^*	ε_{∞}^*
Set 1	1.20	1.61	0.77	0.42	1.55	3.80
Set 2	1.09	1.74	0.70	0.46		
Set 3	1.08	1.89	0.69	0.50		
Set 4	1.11	2.13	0.72	0.56		
Set 5	1.23	2.53	0.79	0.66		
Set 6	1.37	2.95	0.88	0.78		

where j refers to each case in the set of (six) inlet BCs, i indicates each of the N grid points of the discretization and macro and micro refers to the macroscopic solution (for each a , b and c) and the space-averaged microscopic solution, respectively. Preliminary evaluation of the error showed that the coefficient c is relatively close to its original value for the clear flow case ($c \approx 1.92$) independent of the BC, and the diffusion coefficients have a relatively large impact on the solution. Based on this preliminary insight, two simulations are carried out for each j -error. In the first one, both a and b are varied from 0.05 to 10 with a step of 0.05 and c is fixed at 1.9. This set of simulations leads to a smaller total error (i.e., sum over all BCs or j in Eq. (21)) for values of a and b lower than 1. Therefore, in the second set of simulations, a and b are varied from 0.025 to 1 with a step of 0.025 and c is varied from 1 to 3 with a step of 0.1.

The objective of this error-minimization study is only to evaluate if the model can fairly predict the space-averaged microscopic behavior with a fixed set of model parameters. Note for instance, that for the problem under study, the diffusion in the streamwise direction may be expected to be of a lower order than source and convective terms. Therefore, this problem may not be the best choice to compute the diffusion coefficients. Additionally, the reader may note that the definition of the error given in Eq. (21) is somewhat arbitrary, and so is the definition of the overall error (Σerror_j). A different choice of these definitions may lead to a slightly different set of optimal values for the model parameters.

5.3.2. Results

Top six rows of Table 3 show the summary of the results obtained using the values of a , b and c (the model parameters) that minimize the error for each BC. The spread of the calculated model parameters is acceptable. Coefficients a and c are largely independent of the BCs ($a = 0.025$ and $c = 1.9$). Coefficient b needs to be between 0.025 and 1.3 to minimize the error depending upon the boundary condition used. Next, an optimal value of b is estimated that would minimize the error for all six different boundary conditions. The overall error (Σerror_j) for $b = 0.85$ is shown in the bottom row of Table 3. The overall error for this set of model parameters for all six sets of BCs is quite small (.0053) and within acceptable limits. Moreover, the error for each set of BCs (error_{jT} in Table 3) for this set of model parameters (bottom row in Table 3; $a = 0.025$, $b = 0.85$ and $c = 1.9$) is not increased by more than 20% compared to the minimum error for that set of BC (second last column in Table 3). This ratio is shown in the last column of Table 3 for each BC. This implies that the solution for all six different inlet BCs is not significantly degraded with a single optimal set of model parameters or, in other words, the solution is not strongly sensitive to the value of this parameter (b) over the range of BCs under consideration.

Macroscopic solutions for k/k_∞ and $\varepsilon/\varepsilon_\infty$ obtained using the optimal set of parameters ($a = 0.025$, $b = 0.875$ and $c = 1.9$) are compared with the microscopic ones in Figs. 5 for the six inlet BCs. Error bars corresponding to a $\pm 10\%$ error with respect to the averaged microscopic solution are also shown. The agreement be-

tween the reference solution and the macroscopic results is fairly good validating the capabilities of the model to predict the macroscopic turbulence quantities. Largest discrepancies are found for BC Set 1 (5a), but the errors even for this worst case are within a 10% error bar.

Although coefficient c was computed to have a value very close to the one used in clear flows, the diffusion coefficients (i.e., a and b) are drastically different from their corresponding values in clear flow. These coefficients are representing the complete mixing process in the REV as an effective diffusion in the streamwise direction and therefore, they are expected to differ from those used in clear flows. Additionally, the relevant equations in the porous media case are dominated by strong source terms (body forces). These aspects help explain the difference found with the clear flow case. However, further studies are needed to fully understand the order of magnitude difference found in coefficients a and b between clear flow and porous media cases.

5.3.3. Complimentary results for additional BCs

Analyses of the model results and its comparisons with the reference results presented in Fig. 5 may suggest that from the macroscopic point of view, all six inlet BCs used are rather similar and close to the equilibrium values. To test if the model developed in Part I can indeed accurately predict the evolution of the turbulence quantities only when their values at the inlet are close to the equilibrium values, the spatial evolution of the macroscopic turbulence quantities reported by Nakayama and Kuwahara [2] for a geometry similar to the one used in this work suggests additional tests of the model. In that study, the inlet macroscopic BCs for the MTKE and MDR are approximately equal to 9.4 and 9.2, respectively (normalized with the fully developed values). These values are much larger than those used for BC Sets 1 through 6 (see Table 2). Therefore, it is of interest to simulate conditions similar to those presented by NK using the present model.

In the porous medium geometry selected for this study, specifying such high macroscopic values at the inlet of the porous medium as the BC is possible only by employing non-physical microscopic values at the inlet of the domain shown in Fig. 3 (i.e., such BCs are not realizable in the geometry simulated in this study for turbulent intensities below 100%). In this case, the microscopic turbulence quantities, k and ε , at the inlet are chosen equal to 10^1 and 10^{-1} (dimensionless, see Appendix A), respectively. These values result in a very high production of TKE and TDR with low sinks. Additionally, the MTKE is dominated by the space-average of the TKE (the dispersive kinetic energy of the flow is negligible). The macroscopic inlet BCs for the k/k_∞ and $\varepsilon/\varepsilon_\infty$ are 3.8 and 7.7, respectively. Fig. 6 shows the comparison of the macroscopic model results (model parameters given in Table 3) with the reference results. The agreement is rather good for both turbulence quantities. The MDR decay rate is very well matched by the model while the MTKE calculated using the macroscopic model decays slightly faster than the reference results but well within acceptable errors. This example validates the capabilities of the model to predict the evolution of the macroscopic turbulence quantities even for inlet conditions that are far from equilibrium values.

5.3.4. Macroscopic turbulent kinetic energy

The MTKE defined in this study includes the dispersive kinetic energy (k_{DISP}) in addition to the space-average of the TKE (k_{NK}). The spatial evolution of these two quantities, normalized with the fully developed MTKE, are shown in Fig. 7 for the six BCs tabulated in Tables 1 and 2. Both quantities, k_{NK} and k_{DISP} , appear to be important at the macroscopic scale. That is, both quantities are of the same order of magnitude and show the same levels of variation with the spatial evolution of the flow. These microscopic results

Table 3
Parameter values for the macroscopic model and errors between microscopic and macroscopic results for each BC.

Boundary conditions	a	b	c	Error_j^*1000	$\text{Error}_j/\text{Error}_{jT}(\%)$
Set 1	0.025	1.3	1.9	1.5	4.3
Set 2	0.025	1.0	1.9	1.0	0.8
Set 3	0.025	0.7	1.9	0.8	0.6
Set 4	0.025	0.25	1.9	0.6	8.3
Set 5	0.025	0.25	1.9	0.5	18.3
Set 6	0.025	0.025	1.9	0.5	19.7
Overall (all six BCs)	0.025	0.875	1.9	5.3	–

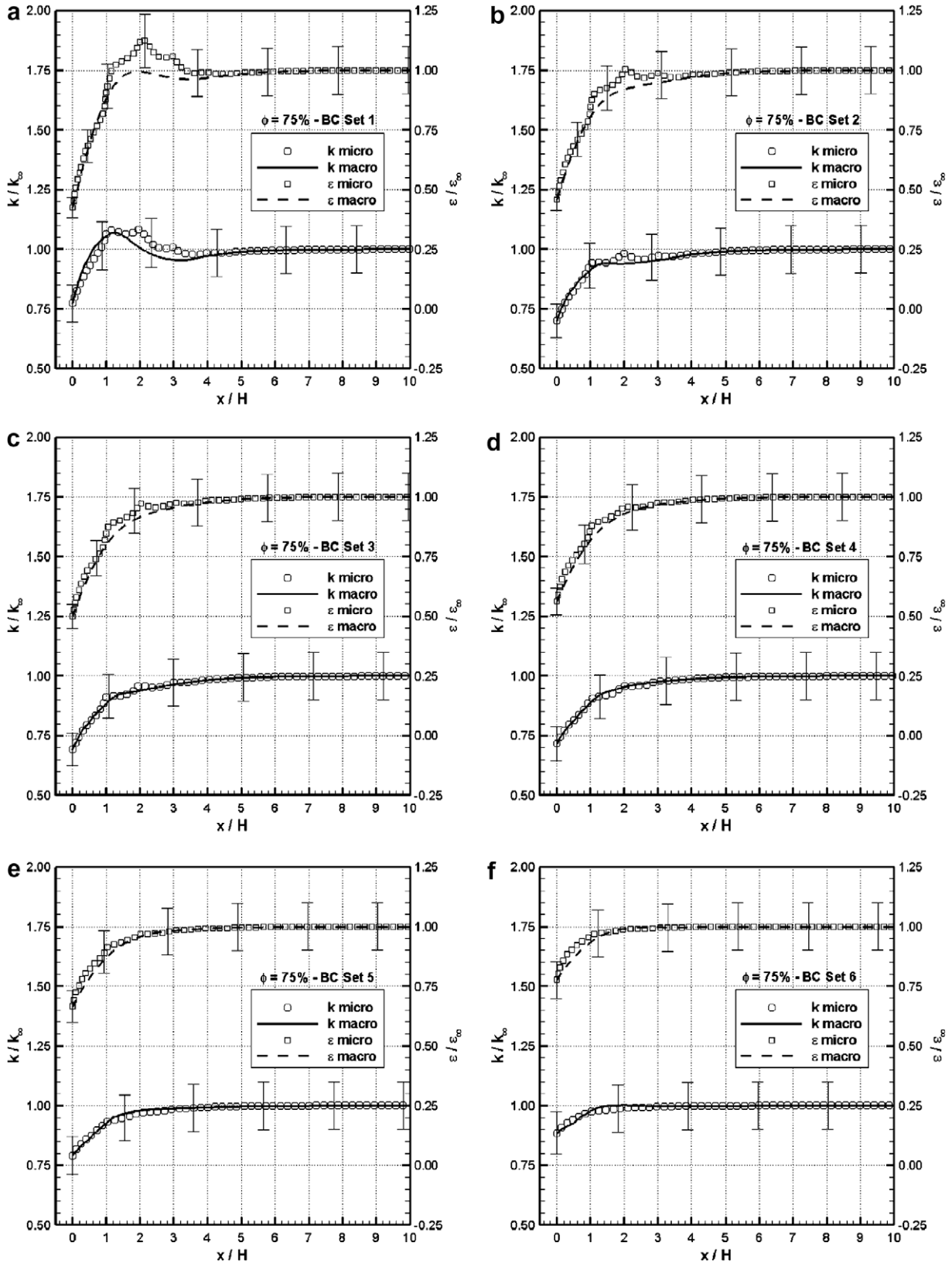


Fig. 5. Streamwise evolution of the MTKE and the MDR calculated using the microscopic and the macroscopic models. Panels (a–f), respectively, show the results for BCs Sets 1–6.

suggest that k_{DISP} , in at least some flows, may be as important as k_{NK} in modeling turbulence at macroscopic scales.

The evolution of k_{DISP} for different BCs (right panel in Fig. 7) suggests that this quantity is larger when the flow has relatively low

eddy viscosity (see Table 1). The inlet BCs that are characterized by relatively low eddy viscosity and therefore, by relatively high values of the local Re number (i.e., considering the effective viscosity as $\nu + \nu_T$), lead to large eddies in the entrance region of the

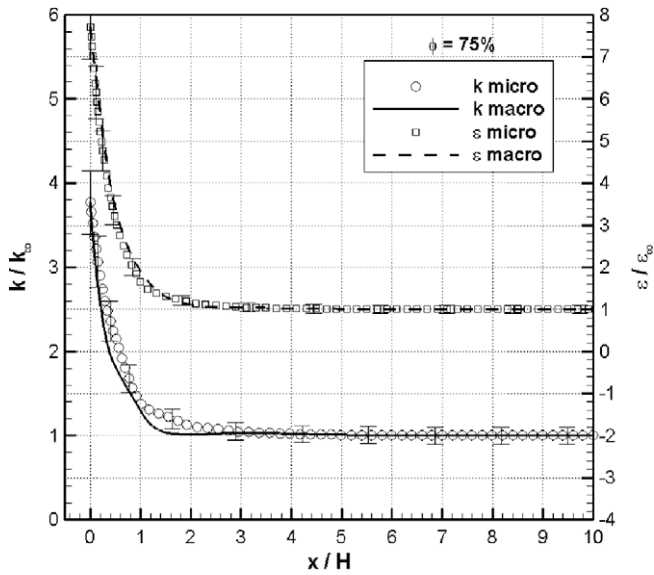


Fig. 6. Streamwise evolution of the MTKE and the MDR calculated using the microscopic and macroscopic models. $Re = 10^4$. Turbulence quantities at the inlet in this case are far from their equilibrium values.

porous medium (see Fig. 4, right panel). It is expected that these flow structures at the microscopic scales enhance the mixing of the flow and therefore, this feature should be represented as an increase in the turbulent mixing at the macroscopic scales. This effect is captured by the quantity k_{DISP} , which enhances the MTKE and therefore the value of the macroscopic eddy viscosity.

It can be argued that the effect of trace of the hydrodynamic dispersion of the mean flow should be modeled separately from the Reynolds stresses. However, as shown by the results presented here, there is a close relationship between the dispersion of the flow and the local (microscopic) turbulence quantities. Large flow dispersion and large velocity gradient contribute to the production of TKE and low eddy viscosities, thus enhancing dispersion. The process of how filtered motions transfer kinetic energy to residual motions was explained in Part I [5]. Obviously, these physical processes are not independent of each other, and thus the results found above should not be surprising.

6. Summary and conclusions

The set of macroscopic equations developed in Part I [5] is validated in this study. The analysis carried out for the case of fully developed macroscopic quantities shows that the macroscopic dissipation rate, defined by the pressure-drop in the REV times the velocity, is a good approximation for the space-average of the microscopic dissipation rate at high Reynolds numbers. A set of optimal model parameter values are determined for developing flow by comparing the results of the macroscopic model with reference data for a set of six different inlet boundary conditions. The comparison of numerical results obtained using the model developed here with averaged microscopic results showed satisfactory agreement. The 75% porosity case was tested using the optimal set of model parameters and showed excellent agreement with reference microscopic results for both turbulence quantities for the entire range of inlet turbulent intensities. The model is tested further with inlet conditions for turbulence quantities that are far from equilibrium values and hence must vary significantly in the developing region of the flow. The turbulence quantities obtained using the same set of optimal model parameters, determined for more “realistic” set of boundary conditions, compared very well with the space-time averaged microscopic results even for such relatively large inlet conditions.

The simple flow (from the macroscopic point of view) studied here proved to be very useful in carrying out the initial steps in the evaluation of the turbulence model for porous media developed in Part I. The fact that the model captures the flow characteristics very well over a large range of inlet boundary conditions suggests that the drag force model in the macroscopic equation for the dissipation rate, originally proposed based on physical insight (see Eq. 48 in Part I), is adequate. The evolution of macroscopic turbulence quantities was validated but, as in existing turbulence models, a more complete study, where the momentum equation is affected by the macroscopic eddy viscosity, is still needed.

In addition to the potential use of the model developed here to simulate turbulence in porous media, the model may also help in developing improved understanding of the approximations introduced in the modeling process. Specifically, the *dispersive kinetic energy* was shown to vary significantly while the flow is developing, representing, in part, the eddies that are found at the microscopic scales. Better understanding of this quantity and its interaction with the space-average of the TKE require further work.

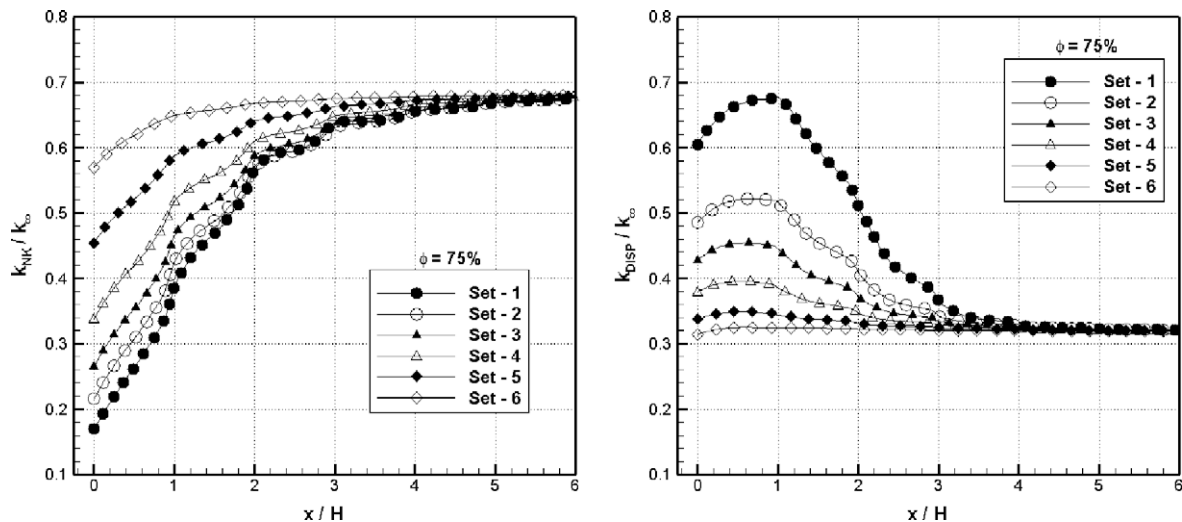


Fig. 7. Spatial evolution of the volume-average of the TKE (left panel) and the dispersive kinetic energy (right panel).

In the present model this quantity is included in the MTKE. The *dispersive kinetic energy* in an alternate approach can be modeled employing an additional transport equation. In this case additional terms describing the transfer of energy between k_{NK} and k_{DISP} need to be included in the model.

Appendix A. Boundary conditions

The choice of boundary conditions (BCs) employed to carry out the microscopic simulations presented in Section 5.1 are explained in detail in this appendix. In addition to the symmetry boundary conditions applied on the horizontal boundaries of the system (Fig. 3), BCs are needed for the inlet and outlet boundaries of the domain. The flow is assumed to be fully developed at the exit. Profiles of U , V , P , k and ε across the exit plane, obtained by simulating the REV of the porous medium with periodic boundary conditions [11] at the inlet and the exit plane, are imposed as BCs at the exit. The length of the porous medium simulated in this study (16H) appears to be sufficient to allow the imposition of the fully developed profiles as BCs at the exit. This assumption was verified by evaluating the results *a posteriori* [11].

The inlet boundary condition is assumed to be a flat profile for both, velocities and turbulence quantities. Due to a mass conservation constraint, the inlet streamwise velocity is chosen to be UH/p , where Up is the flow rate imposed at the exit. Dirichlet boundary conditions are imposed at the inlet for the microscopic turbulence quantities. Simulations are carried out with different levels of turbulence at the inlet. The use of different inlet boundary conditions for the turbulence quantities is motivated by the fact that different levels of turbulence at the inlet affect the flow distribution inside the porous medium and thus lead to different BCs for the macroscopic turbulence quantities. Similar studies are common for instance in the backward-facing step problem in which the turbulence intensity at the inlet affects the flow distribution [18]. The values of the turbulence quantities at the inlet are chosen to cover a large range of turbulence intensities. The value of the TKE is chosen as $k = 3/2l^2$ to represent the turbulence intensity of the flow assuming isotropic turbulence, where l is the turbulence intensity and k has been made dimensionless with U . To specify the turbulence dissipation rate at the inlet, a length scale is needed or a value for the inlet eddy viscosity needs to be assumed. This represents a drawback when the k - ε model is employed because this quantity is in general not known or not measured in experiments (see for instance Wilcox [19]). The TDR is estimated as $\varepsilon \approx 4/10(\mathcal{L}/\mathcal{L}_{11})k^{3/2}$ ([10], following the selection of $\mathcal{L} = p$). Here

\mathcal{L} is the length scale of the problem and \mathcal{L}_{11} is the longitudinal integral length scale or the length scale of the energy-containing eddies. As a rough estimate, $\mathcal{L}/\mathcal{L}_{11} \approx 2$ is used [10]. Therefore, in this study, the dimensionless TDR at the inlet is assumed to be $\varepsilon \approx k^{3/2}$. Note that each set in Table 1 represents a different “level” of turbulence intensity and eddy viscosity, where Set 2 corresponds to a higher level of turbulence intensity than Set 1, and so on.

References

- [1] F. Kuwahara, Y. Kameyama, S. Yamashita, A. Nakayama, Numerical modeling of turbulent flow in porous media using a spatially periodic array, *J. Porous Media* 1 (1998) 47–55.
- [2] A. Nakayama, F. Kuwahara, A macroscopic turbulence model for flow in a porous medium, *J. Fluids Eng.* 121 (1999) 427–433.
- [3] M.H.J. Pedras, M.J.S. de Lemos, Macroscopic turbulence modeling for incompressible flow through undeformable porous media, *Int. J. Heat Mass Transfer* 44 (2001) 1081–1093.
- [4] M.J.S. de Lemos, *Turbulence in Porous Media Modeling and Applications*, Elsevier, 2006.
- [5] F.E. Teruel, Rizwan-uddin, A new turbulence model for porous media flows. Part I: Constitutive equations and model closure, *Int. J. Heat Mass Transfer* (2009), doi:10.1016/j.ijheatmasstransfer.2009.04.017.
- [6] M. Kaviany, *Principles of Heat Transfer in Porous Media*, Springer-Verlag, 1991.
- [7] F. Kuwahara, A. Nakayama, H. Koyama, Numerical modeling of heat and fluid flow in a porous medium, *Proceeding of 10th International Heat Transfer Conference*, vol. 5, 1994, pp. 309–314.
- [8] F. Kuwahara, T. Yamane, A. Nakayama, Large eddy simulation of turbulent flow in porous media, *Int. Commun. Heat Mass Transfer* 33 (2006) 411–418.
- [9] B.V. Antohe, J.L. Lage, A general two-equation macroscopic turbulence model for incompressible flow in porous media, *Int. J. Heat Mass Transfer* 40 (1997) 3013–3024.
- [10] S.B. Pope, *Turbulent Flows*, Cambridge University Press, 2000.
- [11] F.E. Teruel, *Macroscopic turbulence modeling and simulation for flow through porous media*, PhD Thesis, University of Illinois, Urbana-Champaign, IL, 2007.
- [12] S.V. Patankar, *Numerical Heat Transfer and Fluid Flow*, Hemisphere (1980).
- [13] B.P. Leonard, A stable and accurate convective modeling procedure based on quadratic upstream interpolation, *Comput. Methods Appl. Mech. Eng.* 19 (1979) 59–98.
- [14] T. Hayase, J.A.C. Humphrey, R. Greif, A consistently formulated QUICK scheme for fast and stable convergence using finite-volume iterative calculation procedures, *J. Comput. Phys.* 98 (1982) 108–118.
- [15] K. Abe, T. Kondoh, Y. Nagano, A new turbulence model for predicting fluid flow and heat transfer in separating and reattaching flows. 1. Flow field calculations, *Int. J. Heat Mass Transfer* 37 (1994) 139–151.
- [16] W.G. Gray, A. Leijnse, R.L. Kolar, C.A. Blain, *Mathematical Tools for Changing Spatial Scales in the Analysis of Physical Systems*, CRC Press, 1993.
- [17] M. Quintard, S. Whitaker, Transport in ordered and disordered porous media. II. Generalized volume averaging, *Transport Porous Media* 14 (1994) 179–206.
- [18] K. Isomoto, S. Honami, The effect of inlet turbulence intensity on reattachment process over a backward-facing step, *J. Fluids Eng.* 111 (1989) 87–92.
- [19] D.C. Wilcox, *Turbulence Modeling for CFD*, DCW Industries Inc., 2004.